Laser Cooling of Nuclear Magnons

Haowei Xu,[1] Guoqing Wang,[1,2] Changhao Li,[1,2,‡] Hua Wang,[1] Hao Tang,[3] Ariel Rebekah Barr,[3] Paola Cappellaro,[1,2,4,*] and Ju Li[1,3,†]

[1]Department of Nuclear Science and Engineering, Massachusetts Institute of Technology, Cambridge, Massachusetts 02139, USA
[2]Research Laboratory of Electronics, Massachusetts Institute of Technology, Cambridge, Massachusetts 02139, USA
[3]Department of Materials Science and Engineering, Massachusetts Institute of Technology, Cambridge, Massachusetts 02139, USA
[4]Department of Physics, Massachusetts Institute of Technology, Cambridge, Massachusetts 02139, USA

(Received 4 September 2022; accepted 3 January 2023; published 9 February 2023)

The initialization of nuclear spin to its ground state is challenging due to its small energy scale compared with thermal energy, even at cryogenic temperature. In this Letter, we propose an optonuclear quadrupolar effect, whereby two-color optical photons can efficiently interact with nuclear spins. Leveraging such an optical interface, we demonstrate that nuclear magnons, the collective excitations of nuclear spin ensemble, can be cooled down optically. Under feasible experimental conditions, laser cooling can suppress the population and entropy of nuclear magnons by more than 2 orders of magnitude, which could facilitate the application of nuclear spins in quantum information science.

DOI: 10.1103/PhysRevLett.130.063602

Introduction.—Physical qubit platforms are one of the foundations of quantum information science and technology. Nuclear spins have long been perceived as ideal quantum information carriers, thanks to their robustness against environmental perturbations and unparalleled coherence time [1,2]. However, the application of nuclear spins is hindered by several challenges, one of which is the initialization problem: For a typical nuclear spin under a 1 T magnetic field, a 99% initialization fidelity by thermal equilibration requires a demanding temperature below 0.1 mK. The initialization of the nuclear spins can be facilitated by the hyperfine interaction with electron spins, using, e.g., dynamic nuclear polarization [3] or optical orientation [4]. But the necessity of ancillary electrons engenders other shortcomings, such as limited applicability only in systems with nonzero electron spins and shortened nuclear spin coherence time [5,6].

Laser cooling of (quasi)-particles, including neutral atoms [7], mechanical modes [8–11], semiconductors [12], and electron magnons [13], has witnessed great success. Optical lasers have also been used to initialize qubit systems, such as electron and nuclear spins (indirectly via the hyperfine interaction) in nitrogen-vacancy centers [14]. If nuclear spins can be cooled down and initialized optically, their applications would be significantly facilitated. However, there is a lack of effective optical interfaces to nuclear spins without ancillary electron spins.

In this work, we first introduce the optonuclear quadrupolar (ONQ) effect, whereby two-color photons can efficiently interact with nuclear spins without the need for ancillary electron spins. Then we describe the properties of nuclear magnons (NMs), which are the collective excitations of a nuclear spin ensemble (NSE) in crystalline solids such as zinc blende GaAs (zbGaAs) [15–18] and have an exceptionally low decay rate down to 0.1 kHz. As the ONQ coupling strength between optical photons and NMs scales with the number of nuclear spins as $\sqrt{N}$, the ONQ effect is suitable for controlling large NSE. Taking advantage of these properties, we demonstrate the laser cooling of the NM via the ONQ effect. From an initial temperature of mK obtainable in dilute refrigerators [19], the population and the entropy of the NM can be simultaneously reduced by more than 2 orders of magnitude under feasible experimental conditions.

Optonuclear quadrupolar effect.—The Hamiltonian of a nucleus with spin $I > \frac{1}{2}$ is $H_n = \gamma_n \boldsymbol{\mathcal{B}} \cdot \boldsymbol{I} + \boldsymbol{I} \cdot \boldsymbol{\mathcal{Q}} \cdot \boldsymbol{I} = \gamma_n \sum_i \mathcal{B}_i I_i + \sum_{ij} \mathcal{Q}_{ij} I_i I_j$, where the first and second terms are the nuclear magnetic (Zeeman) and nuclear electric quadrupole interactions, respectively. γ_n is the nuclear gyromagnetic ratio, $\boldsymbol{\mathcal{B}}$ is the magnetic field, $\boldsymbol{I}$ is the nuclear spin operator, and $i, j = x, y, z$ are Cartesian indices. The Zeeman interaction comes from the nuclear magnetic dipole. In nonspherical nuclei, an electric quadrupole moment $\mathscr{q}$ also arises as the leading order electric moment when one performs the multipole expansion (the nuclear electric dipole is zero because of inversion symmetry, see, e.g., Chap. 3 in Ref. [20]). The interaction between the nuclear electric quadrupole moment and the electric field gradient (EFG) at the site of the nucleus leads to the nuclear quadrupole interaction $\mathcal{Q}_{ij} \equiv e\mathscr{q}\mathcal{V}_{ij}/[2I(2I-1)]$, where $\mathcal{V}_{ij}$ is the EFG operator.

Traditional techniques for controlling nuclear spins (e.g., nuclear magnetic resonance) rely on modulating the Zeeman interaction using microwave magnetic fields. It is also possible to control nuclear spins by modulating the EFG through electric interaction with the nuclear spin.

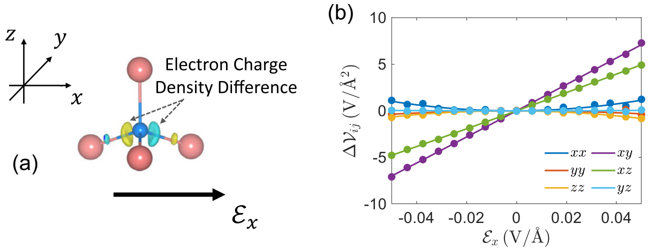

FIG. 1. The ONQ effect in zinc-blende GaAs. (a) Yellow (green) bubbles denote positive (negative) changes in electron charge density when an electric field $\mathcal{E}_x$ is applied. Pink (blue) spheres are Ga (As) atoms. (b) $\Delta\mathcal{V}_{ij}$ at the site of As nuclei as a function of $\mathcal{E}_x$.

Particularly, one can use external electric field(s) to drive the orbital motion of electrons, so that there is a change $\Delta\mathcal{V}$ in the EFG generated by electrons. Under two-color electric fields $\mathcal{E}_{p(q)}(t) = \mathcal{E}_{p(q)}e^{i\omega_{p(q)}t}$, the electron cloud oscillates in real space with a frequency $\omega_p - \omega_q$ [Fig. 1(a)]. Consequently, the EFG generated by electrons and thus the nuclear electric quadrupole interaction will also have an oscillating part with frequency $\omega_p - \omega_q$, which can match nuclear spin energies. This is what we call the ONQ effect. The ONQ effect is a cousin process of Raman scattering or difference frequency generation (DFG) [21]. In Raman (DFG), the oscillation of electrons leads to the emission of phonons (photons) at the difference-frequency $\omega_p - \omega_q$; In ONQ, the oscillation of electrons results in the oscillations of the nuclear electric quadrupole interaction at the difference frequency.

Formally, the oscillating nuclear quadrupole interaction can be expressed as

$$H_{\mathrm{ONQ}} = \sum_{ij} \mathcal{D}_{ij}^{pq}(\omega_p - \omega_q; \omega_p, -\omega_q)\mathcal{E}_p(\omega_p) \times \mathcal{E}_q(-\omega_q) I_i I_j e^{\mathrm{i}(\omega_p - \omega_q)t} + \mathrm{H.c.}, \tag{1}$$

where H.c. stands for Hermitian conjugate. Terms with frequencies ω_p, ω_q, and $\omega_p + \omega_q$ are far off-resonance with nuclear spin dynamics and are omitted. $\mathcal{D}_{ij}^{pq} \equiv \partial^2 \mathcal{Q}_{ij}/\partial\mathcal{E}_p\partial\mathcal{E}_q$ is the second-order response function of the quadrupole tensor. In the single-particle approximation, one has [22]

$$\begin{aligned}&\mathcal{D}_{ij}^{pq}(\omega_p - \omega_q; \omega_p, -\omega_q)\\ &= \frac{e^3 \mathcal{q}}{2I(2I-1)} \sum_{mnl} \frac{[\mathcal{V}_{ij}]_{mn}}{E_{mn} - \hbar(\omega_p - \omega_q)}\\ &\times \left\{ \frac{f_{lm}[r_p]_{nl}[r_q]_{lm}}{E_{ml} - \hbar\omega_p} - \frac{f_{nl}[r_q]_{nl}[r_p]_{lm}}{E_{ln} - \hbar\omega_p} \right\} + (p \leftrightarrow q),\end{aligned} \tag{2}$$

where $(p \leftrightarrow q)$ indicates the exchange of the p and q subscripts, which symmetrizes the ω_p and ω_q fields. m, n, l label the electronic states, E_{mn} and f_{mn} are the energy and occupation differences between two electronic states $|m\rangle$ and $|n\rangle$. Meanwhile, $[r_i]_{mn} \equiv \langle m|r_i|n\rangle$ is the position operator, and $[\mathcal{V}_{ij}]_{mn} = (e/4\pi\varepsilon_0)\langle m|(3r_ir_j - \delta_{ij}r^2)/r^5|n\rangle$ is the EFG operator of the electrons, with ε_0 being the vacuum permittivity.

Notably, electron spin operators do not explicitly appear in Eq. (2), corroborating that the ONQ effect does not need ancillary electron spin. Besides, the light frequency $\omega_{p(q)}$ only appears in the denominators. Hence, the $\mathcal{D}$ tensor is insensitive to $\omega_{p(q)}$ when they are not close to the electron band gap E_g, leading to flexibility in choosing $\omega_{p(q)}$; moreover, all electrons contribute to the ONQ response, as indicated by the summation over (m, n, l) indices. When $\omega_{p(q)} > E_g$, electrons can do resonant interband transitions. When $\omega_{p(q)} < E_g$, the electron interband transitions are virtual. We will consider $\omega_{p(q)} < E_g$ to avoid resonant one-photon absorptions (Sec. 3 of Ref. [23], which also cites Refs. [1,2,24–64]).

Magnitude of the $\mathcal{D}$ tensor.—For an order-of-magnitude estimation of the $\mathcal{D}$ tensor, we use $\langle m|(3r_ir_j - \delta_{ij}r^2)/r^5|n\rangle \approx 1/a_0^3$ and $[r_i]_{mn} \approx a_0$ in Eq. (2). Here a_0 is the Bohr radius, which is also approximately half the bond length in typical materials. In addition, we only consider the (m, n, l) pair that satisfies $E_{mn} = E_{ml} = E_g$, which makes the major contribution to $\mathcal{D}$ when $\omega_{p(q)} < E_g$. Then, one has $\mathcal{D} \sim [g_S/2I(2I-1)](e^4\mathcal{q}/4\pi\varepsilon_0 a_0)[1/E_g(E_g - \omega_p)]$ with $g_S = 2$ the electron spin degeneracy. As an example, this estimate yields $\mathcal{D} \sim 0.24 \times [2\pi \cdot \mathrm{Hz}/(\mathrm{MV/m})^2]$ for ^{75}As nuclei in zbGaAs when $E_g - \omega_p = 0.2$ eV. The $\mathcal{D}$ tensor can also be evaluated using density functional theory (DFT, Sec. 4.1 of Ref. [23]). We apply a static electric field $\mathcal{E}$ and calculate the change in EFG $\Delta\mathcal{V}$. Then $\mathcal{D}$ in the static limit $(\omega_p = \omega_q = 0)$ can be obtained by fitting the $\Delta\mathcal{V}$-$\mathcal{E}$ curve [Fig. 1(b), 1 V/Å $= 10^4$ MV/m], yielding $\mathcal{D}(0; 0, 0) \approx 0.20 \times [2\pi \cdot \mathrm{Hz}/(\mathrm{MV/m})^2]$ for ^{75}As nuclei in zbGaAs, in reasonable agreement with the analytical estimate above. Notably, due to the tetrahedral symmetry of zbGaAs, one has $\mathcal{Q} = 0$ when $\mathcal{E} = 0$. However, $\mathcal{D}$ is nonzero. The validity of the estimation of the $\mathcal{D}$ tensor is assessed in Sec. 4.2 of Ref. [23]. We will adopt $\mathcal{D} = 0.2 \times [2\pi \cdot \mathrm{Hz}/(\mathrm{MV/m})^2]$ hereafter. For a single nuclear spin (Sec. 2.5 of Ref. [23]), the ONQ coupling strength is only 20 Hz when $\mathcal{E}_p = \mathcal{E}_q = 10$ MV/m. Fortunately, as we will show later, the collective ONQ coupling of an NSE can be boosted by a $\sqrt{N}$ factor. Hence, we will focus on NSE hereafter.

Properties of nuclear magnons.—In analogy with electronic spin magnons [64,65], nuclear spin magnons are collective excitation modes of nuclear spins. For brevity, we assume the nuclei are of the same species. The Hamiltonian of an NSE is $\mathcal{H} = \sum_\alpha(\gamma_n \boldsymbol{I}^\alpha \cdot \boldsymbol{\mathcal{B}} + \boldsymbol{I}^\alpha \cdot \boldsymbol{\mathcal{Q}} \cdot \boldsymbol{I}^\alpha) + \sum_{\alpha\beta} \boldsymbol{I}^\alpha \cdot \boldsymbol{\mathcal{J}}^{\alpha\beta} \cdot \boldsymbol{I}^\beta$, where $\boldsymbol{\mathcal{J}}^{\alpha\beta}$ describes the interaction between two nuclear spins α and β. The spin operators $\boldsymbol{I}^\alpha$ can be converted to NM creation (annihilation) operators $a_{\boldsymbol{k}}^\dagger$ $(a_{\boldsymbol{k}})$ with $\boldsymbol{k}$ being the nuclear magnon

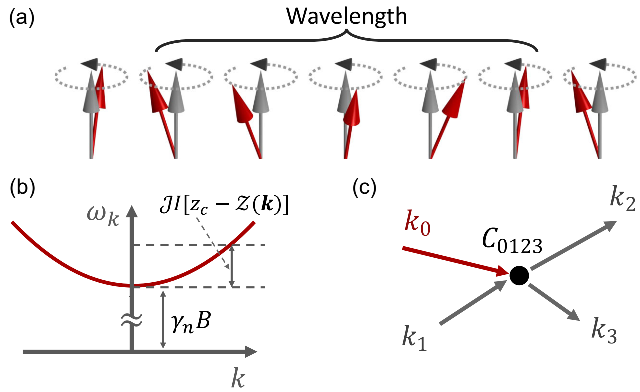

FIG. 2. (a) A semiclassical one-dimensional illustration of the NM mode. (b) Band dispersion of the NMs (not to scale). One has $\gamma_n \mathcal{B} \gg \mathcal{J}I[z_c - \mathcal{Z}(\boldsymbol{k})]$. (c) Illustration of the four-NM scattering process.

wavevector (Sec. 1 of Ref. [23]). Figure 2(a) shows a semiclassical one-dimensional illustration of the NM. Each nuclear spin precesses around its ground state, and the phase of the precession is $e^{i\boldsymbol{k}\cdot\boldsymbol{r}_\alpha}$ with $\boldsymbol{r}_\alpha$ the location of the αth nucleus, so the wavelength is $\lambda = 2\pi/|\boldsymbol{k}|$. This resembles the phonons, whereby the atomic vibrations have a $e^{i\boldsymbol{k}\cdot\boldsymbol{r}_\alpha}$ phase factor.

In the basis of $a_{\boldsymbol{k}}^\dagger$ $(a_{\boldsymbol{k}})$, $\mathcal{H}$ can be decomposed as $\mathcal{H} = \mathcal{H}^{(2)} + \mathcal{H}^{(3)} + \mathcal{H}^{(4)} + \cdots$, where $\mathcal{H}^{(\zeta)}$ contains ζ NM annihilation or creation operators (Sec. 1.2 of Ref. [23]). The quadratic term, $\mathcal{H}^{(2)} = \sum_{\boldsymbol{k}} \omega_{\boldsymbol{k}} a_{\boldsymbol{k}}^\dagger a_{\boldsymbol{k}}$, sets the NM frequency $\omega_{\boldsymbol{k}}$. Higher-order terms such as $\mathcal{H}^{(3)}$ and $\mathcal{H}^{(4)}$, which arise from the $\mathcal{J}$ and $\mathcal{Q}$ terms, correspond to multi-NM interactions and lead to the relaxation of NMs [24]. We will set $\mathcal{Q} = 0$, suitable for GaAs. We also assume a nearest-neighbor Heisenberg interaction $\mathcal{J}_{ij}^{\alpha\beta} = \mathcal{J}\delta_{\langle\alpha\beta\rangle}\delta_{ij}$, where δ_{ij} is the Kronecker delta, and $\delta_{\langle\alpha\beta\rangle}$ enforces α and β to be nearest neighbors. These approximations would not change the order-of-magnitude of the results below (Section 1. 1 of Ref. [23]). Then, one has

$$\omega_{\boldsymbol{k}} = \gamma_n \mathcal{B} + \mathcal{J}I[z_c - \mathcal{Z}(\boldsymbol{k})], \tag{3}$$

where z_c is the coordination number, while $\mathcal{Z}(\boldsymbol{k})$ depends on the lattice structure and is on the order of unity (Sec. 1. 1 of Ref. [23]). Notably, the NM bandwidth ($\mathcal{J}I \sim$ kHz) is much smaller than $\gamma_n \mathcal{B}$ (above MHz when $\mathcal{B}$ is on the order of Tesla), and thus one has $\omega_{\boldsymbol{k}} \approx \omega_0 \equiv \gamma_n \mathcal{B}$. The subscript 0 denotes the near-Γ-point NM mode ($\boldsymbol{k}_0 \approx 0$), which can interact with optical photons and will be the focus henceforth.

The relaxation rate κ_0 of the near-Γ-point NM is a crucial parameter in the laser cooling processes, as we will show below. Because of the small NM bandwidth, three-NM scatterings always violate the conservation of energy, and thus cannot lead to NM relaxation. The leading-order contribution to NM relaxation comes from four-NM scatterings described by $\mathcal{H}^{(4)} = \sum_{0123} C_{0123} a_0 a_1 a_2^\dagger a_3^\dagger + \text{H.c.}$ [the $\boldsymbol{k}_0 + \boldsymbol{k}_1 \to \boldsymbol{k}_2 + \boldsymbol{k}_3$ scattering, Fig. 2(c)]. Here $l = 1$, 2, 3 label three other NMs interacting with the near-Γ-point NM ($l = 0$). The four-NM coupling strength C_{0123} depends on $\mathcal{J}$. Note that $\mathcal{H}^{(4)}$ also contains other terms such as $a_0 a_1^\dagger a_2^\dagger a_3^\dagger$, which are excluded because they violate energy conservation. The relaxation rate in 3D crystal due to four-NM scatterings is $\kappa_0^{(4)} \approx (\pi/2)(3/4\pi)^{\frac{4}{3}}(\mathcal{J}/I\hbar)n_0(n_0+1)$. Notably, the relaxation rate depends on $\mathcal{J}$ and I, which are, respectively, the internuclear interaction strength and the nuclear angular momentum. Specifically, one has $\kappa_0^{(4)} \lesssim [0.1 \sim 1]$ kHz when $n_0 \sim 1$. We set the total NM relaxation rate as $\kappa_0 = \kappa_0^{(4)}$ henceforth, as contributions from higher-order terms $\mathcal{H}^{(\zeta>4)}$ are minor (Sec. 1.2 of Ref. [23], see also Refs. [60,66,67]).

ONQ interaction of nuclear magnons.—Next, we discuss the collective ONQ interaction between optical photons and NMs. To achieve a laser cooling effect, the system is put in an optical cavity resonant with the ω_q photon and is pumped with the ω_p laser. Hence, we second quantize the ω_q photon and treat the ω_p laser as a classical field. The conservation of energy enforces $\omega_q = \omega_p \pm \omega_0$. Specifically, an optical photon with shifted frequency $\omega_h = \omega_p + \omega_0$ ($\omega_l = \omega_p - \omega_0$) is emitted when an NM is annihilated (created), which can be described by (Sec. 1.3 of Ref. [23])

$$\mathcal{H}_{\text{ONQ}} = \mathcal{G}_h b_h^\dagger a_0 + \mathcal{G}_l b_l^\dagger a_0^\dagger + \text{H.c.}, \tag{4}$$

where $b_{h(l)}^\dagger$ is the creation operator of the $\omega_{h(l)}$ photon, and

$$\mathcal{G}_{h(l)} \equiv g\sqrt{N}\mathcal{E}_p \mathcal{E}_{h(l)}^{\text{zpf}} \tag{5}$$

is the collective ONQ coupling strength for NMs with $g \sim \mathcal{D}_{ij}^{pq} \approx 0.2 \times [2\pi \cdot \text{Hz}/(\text{MV/m})^2]$. $\mathcal{E}_{h(l)}^{\text{zpf}}$ is the zero-point field strength of the $\omega_{h(l)}$ photon. Remarkably, $\mathcal{G}_{h(l)}$ is enhanced by a $\sqrt{N}$ factor, similar to the collective coupling between photons and Dicke atomic states or phonons [68,69]. This $\sqrt{N}$ factor indicates that the ONQ effect is suitable for controlling large NSE, which can have sizable interaction with a single cavity photon even if the pumping field $\mathcal{E}_p$ is mild.

Laser cooling mechanism.—The possible transitions of the NM mode under the ω_p laser are illustrated in the inset of Fig. 3(c). Green (red) arrows correspond to the first (second) term in Eq. (4). Efficient laser cooling requires $\mathcal{G}_h \gg \mathcal{G}_l$ [68], which can be realized by using an optical cavity resonant with the ω_h photon, whereby one has $\mathcal{E}_h^{\text{zpf}} = \sqrt{(\hbar\omega_h/2\varepsilon_0 V_h)}$ with V_h the mode volume of the ω_h cavity. The solid green arrows indicate the $\omega_p + \omega_0 \to \omega_h$ process, which annihilates and cools down the NMs. The reverse $\omega_h \to \omega_p + \omega_0$ transition (dashed green arrows) creates NMs and is the back-heating effect. Fortunately, the back heating can be suppressed by keeping the population of the ω_h photon small (ideally zero) via a thermal energy much lower than ω_h. This cooling mechanism is similar to the anti-Stokes cooling of phonons [8–11,68].

In the rotating frame of ω_p, the Hamiltonian of the combined system of ω_h photons and NMs is

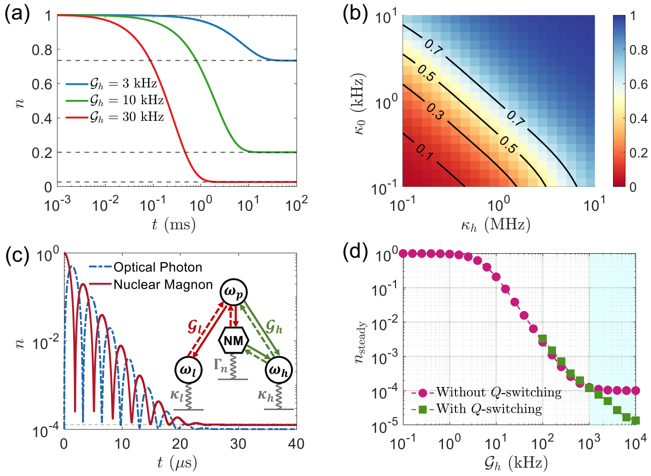

FIG. 3. Laser cooling dynamics. The initial NM population is $n_{\mathrm{th}} = 1$. (a) Time evolution of n_0 in the weak-coupling regime. (b) n_0^{steady} as a function of κ_0 and κ_h in the weak-coupling regime. $\mathcal{G}_h = 10$ kHz. (c) Time evolution of n_0 and n_h in the strong coupling regime. $\mathcal{G}_h = 1$ MHz. Inset of (c) shows possible transitions of the NMs. Circles denote optical photons or lasers with frequencies marked inside. The hexagon denotes the NM. Green and red arrows denote ONQ transitions. Gray wavy lines denote coupling with the heat bath. (d) n_0^{steady} as a function of $\mathcal{G}_h$. The red (green) curve denotes laser cooling without (with) Q switching of the optical cavity. The cyan-shaded area corresponds to the strong-coupling regime. In (a), (c), (d), $\kappa_0 = 0.1$ kHz and $\kappa_h = 1$ MHz are used.

$$\mathcal{H}_C = \omega_0 a_0^\dagger a_0 + (\omega_h - \omega_p) b_h^\dagger b_h + (\mathcal{G}_h b_h^\dagger a_0 + \mathrm{H.c.}). \quad (6)$$

We further assume $\omega_h = 1$ eV and $N/V_h \approx \rho_n$. Here ρ_n is the number density of the nuclei. In solid-state systems, ρ_n can reach $10^{28} \sim 10^{29}$ m^{-3} (for example, one has $\rho \approx 4.2 \times 10^{28}$ m^{-3} for As in zbGaAs). For clarity, we will use $\rho_n = 10^{28}$ m^{-3} hereafter. This leads to $\mathcal{G}_h[\mathrm{kHz}] \approx 1.9 \times \mathcal{E}_p[\mathrm{MV/m}]$, that is, a 1 MV/m pumping field (intensity ≈ 1.3 mW $\cdot$ μm^{-2}) leads to a collective ONQ coupling strength of 1.9 kHz. In practice, much higher laser power above tens of watts can be obtained [70]. Note that $\mathcal{G}_h$ scales as $\sqrt{N/V_h}$, which is the achievable number density ρ_n in the cavity volume V_h (Sec. 3.1 of Ref. [23]).

Laser cooling dynamics.—To demonstrate the laser cooling dynamics, we numerically solve the master equation

$$\frac{\partial \rho}{\partial t} = i[\rho, \mathcal{H}_C] + \kappa_h \xi[b_h]\rho + \kappa_0 (n_{\mathrm{th}} + 1)\xi[a_0]\rho + \kappa_0 n_{\mathrm{th}} \xi[a_0^\dagger]\rho, \quad (7)$$

where ρ is the density matrix of the total system. The Lindblad operator for a given operator o is $\xi(o) = o\rho o^+ - \frac{1}{2}(o^+ o \rho + \rho o^+ o)$. The dissipation rate of the ω_h photon is $\kappa_h = \omega_h / Q_h$ with Q_h the quality factor of the ω_h cavity. $n_{\mathrm{th}} = [\exp(\omega_0/k_B T) - 1]^{-1}$ is the thermal population of the NM mode at temperature T. Considering that ω_0 can be tens of MHz under a magnetic field of 1 T, while T can reach mK in a dilution refrigerator, we fix $n_{\mathrm{th}} = 1$ hereafter. It is also possible to start from a higher temperature and larger n_{th}, but this would make κ_0 larger and the laser cooling less efficient. The thermal population of the ω_h photon is ignored since $\omega_h \gg k_B T$.

The laser cooling behavior is characterized by two parameters $\mathcal{G}_h/\kappa_0$ and $\mathcal{G}_h/\kappa_h$. κ_0 is usually in the sub-kHz range, while $\mathcal{G}_h$ can be well above 1 kHz. Hence, we are in the "strong-coupling" ($\mathcal{G}_h/\kappa_0 \gtrsim 1$) regime regarding NM dissipations. Meanwhile, κ_h can be kept below MHz considering that $Q_h \gtrsim 10^{10}$ has been realized [71–73]. The photon decay rate is analyzed in Sec. 3.3 of Ref. [23], where we show that $\kappa_h = 1$ MHz can be reached if two-photon absorption is avoided. We first fix $\kappa_0 = 0.1$ kHz and $\kappa_h = 1$ MHz. In Fig. 3(a), the time evolution of the NM population $n_0(t)$ is plotted for $\mathcal{G}_h$ in the weak-coupling ($\mathcal{G}_h/\kappa_h \ll 1$) regime. $n_0(t)$ monotonically decays with time, until reaching a steady-state value $n_0^{\mathrm{steady}} = n_{\mathrm{th}}\kappa_0\kappa_h/(4\mathcal{G}_h^2 + \kappa_0\kappa_h)$ [dashed line in Fig. 3(a), see Sec. 2.2 of Ref. [23] and Ref. [68]]. With $\mathcal{G}_h = 10$ kHz (30 kHz), one has $n_0^{\mathrm{steady}}/n_{\mathrm{th}} \approx 0.20$ (0.027). Remarkably, the von Neumann entropy of the NM mode is suppressed as well. The entropy of the final steady state is close to that of a thermal state with a population of n_0^{steady} (Sec. 2.3 of Ref. [23]). Then, we fix $\mathcal{G}_h = 10$ kHz. n_0^{steady} as a function of κ_0 and κ_h is shown in Fig. 3(b). A sizable cooling effect exists even when $\kappa_0 = 1$ kHz and $\kappa_h = 1$ MHz.

Next, we set $\mathcal{G}_h = 1$ MHz [Fig. 3(c)] to demonstrate the laser cooling behavior in the strong-coupling regime. Note that this requires a strong pumping field $\mathcal{E}_p \sim 10^3$ MV/m, which can be challenging in practice. In this strong-coupling regime, there is a swap process between the NM and the ω_h photon with a frequency of $2\mathcal{G}_h$, while the total population ($n_0 + n_h$) drops with an envelope function $e^{-\bar{\kappa}t}$. The overall decay rate is $\bar{\kappa} \approx \frac{1}{2}(\kappa_0 + \kappa_h)$, because approximately the NM and the ω_h photon mode each exist for half of the time t during the swap process. Finally, n_0^{steady} reaches $\sim 10^{-4}$. Interestingly, when $\mathcal{G}_h/\kappa_h \gtrsim 1$, further increasing $\mathcal{G}_h$ does not improve the cooling effect. Instead, n_0^{steady} is almost a constant $n_{\mathrm{th}}\kappa_0/\kappa_h$ due to the back-heating effect [red curve in Fig. 3(d)]. Similar effects have also been observed in the case of optical cooling of phonons [74–76]. This limitation can be circumvented by Q switching [30] (Sec. 2.4 of Ref. [23]). This would minimize the back-heating effect, and n_0^{steady} can be further suppressed when $\mathcal{G}_h/\kappa_h \gtrsim 1$ [green curve in Fig. 3(d)].

In summary, we introduce the ONQ effect, which can efficiently couple optical photons and nuclear spins. We demonstrate the laser cooling of NMs via the ONQ effect. The NM cooling process could be detected by monitoring the emission of cavity photons, and the occupation number reached could be measured by the dispersive frequency shift induced on a detuned anharmonic cavity (Sec. 3.4 of Ref. [23]). Since laser cooling suppresses both the population and the entropy of the NM mode, it could facilitate potential applications of nuclear spins, especially those based on the interface between nuclear spins and optical photons.

This work was supported by an Office of Naval Research MURI through Grant No. N00014-17-1-2661. J. L. and A. B. also acknowledge support by DTRA (Award No. HDTRA1-20-2-0002) Interaction of Ionizing Radiation with Matter (IIRM) University Research Alliance (URA). The calculations in this work were performed in part on the Texas Advanced Computing Center (TACC) and MIT Engaging cluster. H. X. thanks Meihui Liu for help in figure production.

*Corresponding author.
pcappell@mit.edu
†Corresponding author.
liju@mit.edu
‡Present address: Global Technology Applied Research, JPMorgan Chase, New York, New York 10017 USA.

[1] M. Steger, K. Saeedi, M. L. W. Thewalt, J. J. L. Morton, H. Riemann, N. V. Abrosimov, P. Becker, and H. J. Pohl, Quantum information storage for over 180 s using donor spins in a 28Si “semiconductor vacuum,” Science **336**, 1280 (2012).

[2] K. Saeedi, S. Simmons, J. Z. Salvail, P. Dluhy, H. Riemann, N. V. Abrosimov, P. Becker, H. J. Pohl, J. J. L. Morton, and M. L. W. Thewalt, Room-temperature quantum bit storage exceeding 39 minutes using ionized donors in silicon-28, Science **342**, 830 (2013).

[3] L. Lumata, Z. Kovacs, C. Malloy, A. Abragam, and M. Goldman, Principles of dynamic nuclear polarisation, Rep. Prog. Phys. **41**, 395 (1978).

[4] M. I. Dyakonov and V. I. Perel, Theory of optical spin orientation of electrons and nuclei in semiconductors, Modern problems in condensed matter sciences Vol. **8** (1984), p. 11.

[5] D. Layden, M. Chen, and P. Cappellaro, Efficient Quantum Error Correction of Dephasing Induced by a Common Fluctuator, Phys. Rev. Lett. **124**, 020504 (2020).

[6] J. J. Pla, K. Y. Tan, J. P. Dehollain, W. H. Lim, J. J. L. L. Morton, F. A. Zwanenburg, D. N. Jamieson, A. S. Dzurak, and A. Morello, High-fidelity readout and control of a nuclear spin qubit in silicon, Nature (London) **496**, 334 (2013).

[7] W. D. Phillips, Nobel lecture: Laser cooling and trapping of neutral atoms, Rev. Mod. Phys. **70**, 721 (1998).

[8] F. Marquardt, J. P. Chen, A. A. Clerk, and S. M. Girvin, Quantum Theory of Cavity-Assisted Sideband Cooling of Mechanical Motion, Phys. Rev. Lett. **99**, 093902 (2007).

[9] I. Wilson-Rae, N. Nooshi, W. Zwerger, and T. J. Kippenberg, Theory of Ground State Cooling of a Mechanical Oscillator Using Dynamical Backaction, Phys. Rev. Lett. **99**, 093901 (2007).

[10] A. D. O’Connell, M. Hofheinz, M. Ansmann, R. C. Bialczak, M. Lenander, E. Lucero, M. Neeley, D. Sank, H. Wang, M. Weides, J. Wenner, J. M. Martinis, and A. N. Cleland, Quantum ground state and single-phonon control of a mechanical resonator, Nature (London) **464**, 697 (2010).

[11] J. Chan, T. P. M. Alegre, A. H. Safavi-Naeini, J. T. Hill, A. Krause, S. Gröblacher, M. Aspelmeyer, and O. Painter, Laser cooling of a nanomechanical oscillator into its quantum ground state, Nature (London) **478**, 89 (2011).

[12] M. Sheik-Bahae and R. I. Epstein, Can Laser Light Cool Semiconductors?, Phys. Rev. Lett. **92**, 247403 (2004).

[13] S. Sharma, Y. M. Blanter, and G. E. W. Bauer, Optical Cooling of Magnons, Phys. Rev. Lett. **121**, 087205 (2018).

[14] M. W. Doherty, N. B. Manson, P. Delaney, F. Jelezko, J. Wrachtrup, and L. C. L. Hollenberg, The Nitrogen-vacancy colour centre in diamond, Phys. Rep. **528**, 1 (2013).

[15] D. A. Gangloff, G. Éthier-Majcher, C. Lang, E. V. Denning, J. H. Bodey, D. M. Jackson, E. Clarke, M. Hugues, C. Le Gall, and M. Atatüre, Quantum interface of an electron and a nuclear ensemble, Science **364**, 62 (2019).

[16] D. M. Jackson, D. A. Gangloff, J. H. Bodey, L. Zaporski, C. Bachorz, E. Clarke, M. Hugues, C. Le Gall, and M. Atatüre, Quantum sensing of a coherent single spin excitation in a nuclear ensemble, Nat. Phys. **17**, 585 (2021).

[17] D. A. Gangloff, L. Zaporski, J. H. Bodey, C. Bachorz, D. M. Jackson, G. Éthier-Majcher, C. Lang, E. Clarke, M. Hugues, C. Le Gall, and M. Atatüre, Witnessing quantum correlations in a nuclear ensemble via an electron spin qubit, Nat. Phys. **17**, 1247 (2021).

[18] J. M. Taylor, C. M. Marcus, and M. D. Lukin, Long-Lived Memory for Mesoscopic Quantum Bits, Phys. Rev. Lett. **90**, 206803 (2003).

[19] F. Pobell, *Matter and Methods at Low Temperatures* (Springer, Berlin, Heidelberg, 2007).

[20] K. S. Krane, *Introductory Nuclear Physics*, 3rd ed. (Wiley, US, 1987).

[21] T. Suhara and M. Fujimura, Difference-frequency generation devices, in *Waveguide Nonlinear-Optic Devices*, Springer Series in Photonics Vol. 11 (Springer, Berlin, Heidelberg, 2003), pp. 237–270 (2003).

[22] H. Xu, H. Wang, J. Zhou, and J. Li, Pure spin photocurrent in non-centrosymmetric crystals: Bulk spin photovoltaic effect, Nat. Commun. **12**, 4330 (2021).

[23] See Supplemental Material at http://link.aps.org/supplemental/10.1103/PhysRevLett.130.063602 for detailed discussions on (1) properties of nuclear magnons; (2) laser cooling dynamics; (3) assessment of the theoretical approaches; and (4) some experimental considerations; also see Refs. [1,2,24–64].

[24] S. M. Rezende, *Fundamentals of Magnonics* (Springer Cham, 2020), Vol. 969.

[25] T. Feng, L. Lindsay, and X. Ruan, Four-phonon scattering significantly reduces intrinsic Thermal conductivity of solids, Phys. Rev. B **96**, 161201 (2017).

[26] X. Yang, T. Feng, J. S. Kang, Y. Hu, J. Li, and X. Ruan, Observation of strong higher-order lattice anharmonicity in Raman and infrared spectra, Phys. Rev. B **101**, 161202 (2020).

[27] J. König and A. Hucht, Newton series expansion of bosonic operator functions, SciPost Phys. **10**, 007 (2021).

[28] L. D. Landau and E. M. Lifshitz, *Statistical Physics* (Elsevier, New York, 2013), Vol. 5.
[29] M. A. Nielsen and I. Chuang, *Quantum Computation and Quantum Information* (Cambridge University Press, Cambridge, England, 2010).
[30] Y. C. Liu, Y. F. Xiao, X. Luan, and C. W. Wong, Dynamic Dissipative Cooling of a Mechanical Resonator in Strong Coupling Optomechanics, Phys. Rev. Lett. **110**, 153606 (2013).
[31] H. Choi, M. Heuck, and D. Englund, Self-Similar Nanocavity Design with Ultrasmall Mode Volume for Single-Photon Nonlinearities, Phys. Rev. Lett. **118**, 223605 (2017).
[32] J. Burris and T. J. McIlrath, Theoretical study relating the two-photon absorption cross section to the susceptibility controlling four-wave mixing, J. Opt. Soc. Am. B **2**, 1313 (1985).
[33] Third-Order Nonlinear Optical Coefficients of Si, and GaAs in the Near-Infrared Spectral Region, in *Proceedings of 2018 Conference on Lasers and Electro-Optics (CLEO), San Jose, CA, 2018* (IEEE, New York, 2018), https://ieeexplore.ieee.org/document/8427144.
[34] T. Holstein and H. Primakoff, Field dependence of theintrinsic domain magnetization of a ferromagnet, Phys. Rev. **58**, 1098 (1940).
[35] M. M. Choy and R. L. Byer, Accurate second-order susceptibility measurements of visible and infrared nonlinear crystals, Phys. Rev. B **14**, 1693 (1976).
[36] Y.-R. Shen, *Principles of Nonlinear Optics* (Wiley, US, 1984).
[37] G. P. Agrawal and R. W. Boyd, *Contemporary Nonlinear Optics* (1992).
[38] D. Peceli, P. D. Olszak, C. M. Cirloganu, S. Webster, L. A. Padilha, T. Ensley, H. Hu, G. Nootz, D. J. Hagan, and E. W. Van Stryland, Three-photon absorption of GaAs and other semiconductors, in *Proceedings of Nonlinear Optics, Kohala Coast, Hawaii* (Optica Publishing Group, 2013), paper NTu1B.6.
[39] M. S. Dresselhaus, *Solid State Physics Part II Optical Properties of Solids* (n.d.), https://web.mit.edu/6.732/www/6.732-pt2.pdf.
[40] I. Esmaeil Zadeh, J. W. N. N. Los, R. B. M. M. Gourgues, V. Steinmetz, G. Bulgarini, S. M. Dobrovolskiy, V. Zwiller, and S. N. Dorenbos, Single-photon detectors combining high efficiency, high detection rates, and ultra-high timing resolution, APL Photonics **2**, 111301 (2017).
[41] V. B. Verma *et al.*, Single-photon detection in the mid-infrared up to 10 μm wavelength using tungsten silicide superconducting nanowire detectors, APL Photonics **6**, 056101 (2021).
[42] P. Arrangoiz-Arriola, E. A. Wollack, Z. Wang, M. Pechal, W. Jiang, T. P. McKenna, J. D. Witmer, R. Van Laer, and A. H. Safavi-Naeini, Resolving the energy levels of a nanomechanical oscillator, Nature (London) **571**, 537 (2019).
[43] I. Schuster, A. Kubanek, A. Fuhrmanek, T. Puppe, P. W. H. H. Pinkse, K. Murr, and G. Rempe, Nonlinear spectroscopy of photons bound to one atom, Nat. Phys. **4**, 382 (2008).
[44] A. Kubanek, A. Ourjoumtsev, I. Schuster, M. Koch, P. W. H. Pinkse, K. Murr, and G. Rempe, Two-Photon Gateway in One-Atom Cavity Quantum Electrodynamics, Phys. Rev. Lett. **101**, 203602 (2008).
[45] R. Kubo, The spin-wave theory of antiferromagnetics, Phys. Rev. **87**, 568 (1952).
[46] P. Giannozzi *et al.*, QUANTUM ESPRESSO: A modular and open-source software project for quantum simulations of materials, J. Phys. Condens. Matter **21**, 395502 (2009).
[47] P. Giannozzi *et al.*, Advanced capabilities for materials modelling with QUANTUM ESPRESSO, J. Phys. Condens. Matter **29**, 465901 (2017).
[48] J. P. Perdew, K. Burke, and M. Ernzerhof, Generalized Gradient Approximation Made Simple, Phys. Rev. Lett. **77**, 3865 (1996).
[49] P. E. Blöchl, Projector augmented-wave method, Phys. Rev. B **50**, 17953 (1994).
[50] R. D. King-Smith and D. Vanderbilt, Theory of polarization of crystalline solids, Phys. Rev. B **47**, 1651 (1993).
[51] R. Resta and D. Vanderbilt, Theory of polarization: A modern approach, in Physics of Ferroelectrics, Topics in Applied Physics Vol. **105** (2007), pp. 31–68.
[52] M. Pfender *et al.*, Protecting a diamond quantum memory by charge state control, Nano Lett. **17**, 5931 (2017).
[53] V. Ivády, I. A. Abrikosov, and A. Gali, First principles calculation of spin-related quantities for point defect qubit research, npj Comput. Mater. **4**, 76 (2018).
[54] Á. Gali, *Ab initio* theory of the nitrogen-vacancy center in diamond, Nanophotonics **8**, 1907 (2019).
[55] M. Ono, J. Ishihara, G. Sato, Y. Ohno, and H. Ohno, Coherent manipulation of nuclear spins in semiconductors with an electric field, Appl. Phys. Express **6**, 033002 (2013).
[56] S. N. Datta and A. Panda, All-temperature magnon theory of ferromagnetism, J. Phys. Condens. Matter **21**, 336003 (2009).
[57] S. Asaad, V. Mourik, B. Joecker, M. A. I. Johnson, A. D. Baczewski, H. R. Firgau, M. T. Mądzik, V. Schmitt, J. J. Pla, F. E. Hudson, K. M. Itoh, J. C. Mccallum, A. S. Dzurak, A. Laucht, and A. Morello, Coherent electrical control of a single high-spin nucleus in silicon, Nature (London) **579**, 205 (2020).
[58] Z. Z. Li, Y. F. Niu, and W. H. Long, Electric dipole polarizability in neutron-rich Sn isotopes as a probe of nuclear isovector properties, Phys. Rev. C **103**, 064301 (2021).
[59] J. R. Johansson, P. D. Nation, and F. Nori, QuTiP: An open-source Python framework for the dynamics of open quantum systems, Comput. Phys. Commun. **183**, 1760 (2012).
[60] S. M. Rezende and R. M. White, Multimagnon theory of antiferromagnetic resonance relaxation, Phys. Rev. B **14**, 2939 (1976).
[61] S. M. Rezende and R. M. White, Spin-wave lifetimes in antiferromagnetic $RbMnF_3$, Phys. Rev. B **18**, 2346 (1978).
[62] C. Kittel and P. McEuen, *Introduction to Solid State Physics* (John Wiley & Sons, New York, 2018).
[63] S. M. Rezende, A. Azevedo, and R. L. Rodriguez-Suarez, Introduction to antiferromagnetic magnons, J. Appl. Phys. **126**, 151101 (2019).
[64] H. Y. Yuan, Y. Cao, A. Kamra, R. A. Duine, and P. Yan, Quantum magnonics: When magnon spintronics meets quantum information science, Phys. Rep. **965**, 1 (2022).
[65] A. V. Chumak, V. I. Vasyuchka, A. A. Serga, and B. Hillebrands, Magnon spintronics, Nat. Phys. **11**, 453 (2015).

[66] T. Feng and X. Ruan, Quantum mechanical prediction of four-phonon scattering rates and reduced thermal conductivity of solids, Phys. Rev. B **93**, 045202 (2016).

[67] S. M. Rezende and R. M. White, Spin-wave lifetimes in antiferromagnetic $RbMnF_3$, Phys. Rev. B **18**, 2346 (1978).

[68] M. Aspelmeyer, T. J. Kippenberg, and F. Marquardt, Cavity optomechanics, Rev. Mod. Phys. **86**, 1391 (2014).

[69] M. J. A. Schuetz, E. M. Kessler, G. Giedke, L. M. K. Vandersypen, M. D. Lukin, and J. I. Cirac, Universal Quantum Transducers Based on Surface Acoustic Waves, Phys. Rev. X **5**, 031031 (2015).

[70] C. B. Hitz, J. J. Ewing, and J. Hecht, *Introduction to Laser Technology* (Wiley, Hoboken, New Jersey, 2012).

[71] S. Probst, A. Tkalčec, H. Rotzinger, D. Rieger, J. M. Le Floch, M. Goryachev, M. E. Tobar, A. V. Ustinov, and P. A. Bushev, Three-dimensional cavity quantum electrodynamics with a rare-earth spin ensemble, Phys. Rev. B **90**, 100404(R) (2014).

[72] H. Goto, K. Ichimura, and S. Nakamura, Experimental determination of intracavity losses of monolithic Fabry-Perot cavities made of $Pr^{3+}:Y_2SiO_5$, Opt. Express **18**, 23763 (2010).

[73] V. Huet, A. Rasoloniaina, P. Guillemé, P. Rochard, P. Féron, M. Mortier, A. Levenson, K. Bencheikh, A. Yacomotti, and Y. Dumeige, Millisecond Photon Lifetime in a Slow-Light Microcavity, Phys. Rev. Lett. **116**, 133902 (2016).

[74] J. M. Dobrindt, I. Wilson-Rae, and T. J. Kippenberg, Parametric Normal-Mode Splitting in Cavity Optomechanics, Phys. Rev. Lett. **101**, 263602 (2008).

[75] I. Wilson-Rae, N. Nooshi, J. Dobrindt, T. J. Kippenberg, and W. Zwerger, Cavity-assisted backaction cooling of mechanical resonators, New J. Phys. **10**, 095007 (2008).

[76] P. Rabl, C. Genes, K. Hammerer, and M. Aspelmeyer, Phase-noise induced limitations on cooling and coherent evolution in optomechanical systems, Phys. Rev. A **80**, 063819 (2009).